

The Disc-Jet Relation in Strong-lined Blazars

Valerio D’Elia^{1,2,3}, Paolo Padovani^{1,4}, Hermine Landt^{1,5}

¹ *Space Telescope Science Institute, 3700 San Martin Drive, Baltimore, MD 21218, USA*

² *Dipartimento di Fisica, II Università di Roma “Tor Vergata”, Via della Ricerca Scientifica 1, I-00133 Roma, Italy*

³ *Osservatorio Astronomico di Roma, Via di Frascati 33, I-00040 Monteporzio, Italy (current address)*

⁴ *ESA Space Telescope Division*

⁵ *Hamburger Sternwarte, Gojenbergsweg 112, D-21029 Hamburg, Germany*

Accepted , Received

ABSTRACT

The relation between accretion disc (thermal emission) and jet (non-thermal emission) in blazars is still a mystery as, typically, the beamed jet emission swamps the disc even in the ultraviolet band where disc emission peaks. In this paper we estimate the accretion disc component for 136 flat-spectrum radio quasars selected from the Deep X-ray Radio Blazar Survey. We do this by deriving the accretion disc spectrum from the mass and accretion rate onto the central black hole for each object, estimated using the emission line widths and the power emitted from the broad line region. We find that non-thermal emission dominates the optical/UV band of our sources. The thermal component, in fact, is, on average, ~ 15 per cent of the total and $\gtrsim 90$ per cent of the objects in the sample have a thermal component < 0.5 of the total luminosity. We then estimate the integrated disc and kinetic jet powers and find that, on average, the disc luminosity is ~ 1 to 20 times the jet power (depending on the uncertainties in the estimation of the latter quantity). A comparison with previous, independent results favours a scenario in which jet and disk powers are of the same order of magnitude. Extraction of energy from a rotating black hole via the “Blandford-Znajek” mechanism fails to explain the estimated jet power in the majority of our sources. Finally, we find that the typical masses for our sources are $\sim 5 \times 10^8 M_\odot$ and that, contrary to previous claims, about one quarter of our radio quasars have relatively small ($< 3 \times 10^8 M_\odot$) black hole mass.

Key words: accretion discs — galaxies: active — galaxies: jets — quasars: emission lines

1 INTRODUCTION

Blazars are probably the most extreme class of Active Galactic Nuclei (AGN) due to their peculiar features: strong, high-frequency, flat radio emission from compact cores, often expanding at superluminal speed (e.g., Jorstad et al. 2001); irregular, rapid variability (e.g., Boettcher 1999); strong radio and optical polarization (e.g., Yuan et al. 2001); and a broad continuum extending to the GeV energies and beyond (e.g., Mukherjee 2001).

The defining features of the blazar class can be explained within the scenario first proposed by Blandford & Rees (1978). Namely, radiation from these sources is likely produced in a relativistic jet of particles with bulk Lorentz factor $\Gamma \sim 10 - 20$; when the jet is observed at small angle, the so-called “beaming” effect is responsible for most of the above features. The spectral energy distribution (SED) of blazars commonly presents a double peak structure (Fosati et al. 1998). The first peak (usually located between the infrared and the UV band) is interpreted as synchrotron

emission from the relativistic electrons in the jet. The same electron population can inverse Compton scatter the synchrotron produced photons (synchrotron self Compton) and photons from the disc or the emission line regions (external Compton) to produce high energy radiation peaking in the X-ray to γ -ray region (Ghisellini 1999).

Among the blazar class, two subclasses can be identified (see Urry & Padovani 1995). The first one is constituted by the Flat Spectrum Radio Quasars (FSRQ). These are very powerful sources (exceeding in some cases $L \sim 10^{47}$ erg s⁻¹) which show strong and broad emission lines. To the second one belong the BL Lacertae objects (BL Lacs), less luminous, and lacking emission lines with equivalent width $\geq 5 \text{ \AA}$.

Due to the strong and relativistically amplified emission from the jet, the thermal contribution from the accretion disc to the total luminosity cannot be in general directly observed in blazars. For this reason the relation between

arXiv:astro-ph/0211147v1 7 Nov 2002

disc and jet is still uncertain for this class of sources (see Celotti, Padovani & Ghisellini 1997 and references therein).

In this paper we try to disentangle the blazar disc and jet components in the optical/UV band. We do this by evaluating masses and accretion rates for a sample of blazars, using these parameters to compute an accretion disc emission model. To this order, information on the accretion disc continuum is required, but that is generally swamped by the beamed jet emission. Therefore, we use the Broad Line Region (BLR) luminosity and relate it to the thermal emission. Thus, we are led to take in account in our analysis only FSRQ sources, which show strong emission lines (although some BL Lacs show some emission lines, these sources are thought to have a very weak, if any, accretion disc component; e.g., Cavaliere & D’Elia 2002).

The paper is organized as follows. In Section 2 we briefly describe the sample from which we selected the sources to be studied. In Section 3 we discuss the method used to evaluate the thermal contribution of the selected sources. In Section 4 we test this method on a sample of radio-quiet quasars. In Section 5 we compute the thermal spectrum for the sources in our sample and we subtract it from the measured spectra, to disentangle the accretion disc emission from the synchrotron one. In Section 6 we evaluate and compare the total thermal and jet powers. In Section 7 we discuss our results while Section 8 summarizes our conclusions. Throughout this paper the values $H_0 = 65 \text{ Km s}^{-1} \text{ Mpc}^{-1}$ and $q_0 = 0.15$ have been adopted and spectral indices are written as $f_\nu \propto \nu^{-\alpha}$.

2 THE SAMPLE

The FSRQ selected for our analysis belong to the Deep X-ray Radio Blazar Survey (DXRBS). The DXRBS has been built by cross-correlating all the serendipitous X-ray sources in the ROSAT database WGACAT (first revision: White, Giommi & Angelini 1995) with a number of radio catalogs (see Perlman et al. 1998 and Landt et al. 2001 for details).

To select blazar candidates among all the radio sources a spectral index cut $\alpha_r \leq 0.7$ was adopted. This is a very efficient way to find blazars because it selects all FSRQ (separated by definition from the Steep Spectrum Radio Quasars at $\alpha_r = 0.5$), basically all BL Lacs, and excludes almost all radio galaxies.

DXRBS is currently the faintest and largest flat-spectrum radio sample with nearly complete (~ 95 per cent) identification, reaching $\sim 50 \text{ mJy}$ at 5 GHz , i.e., radio fluxes $10 - 20$ times fainter than previously published blazar samples. As of July 2002, the DXRBS includes 198 FSRQ; of these, we choose the 136 sources for which the BLR luminosity, L_{BLR} , was available (Landt et al., in preparation). Among these, 113 are newly identified sources with available optical spectra. The remaining 23 FSRQ were previously known, and for these sources we do not have optical or UV spectra, although we have BLR fluxes. Therefore, we calculate mass, accretion rate and total thermal power for all sources (see Sect. 3 and 6), while for the former ones we also disentangle the luminosity components in the optical band (see section 5).

The classification and spectra of most of the sources used in this paper are given in Perlman et al. (1998) and

Landt et al. (2001). The remaining sources will be included in future DXRBS papers, currently in preparation. Line parameters (fluxes and widths) will be presented by Landt et al., in preparation.

3 THE METHOD

In order to reproduce the thermal contribution to the total emission of blazars we need an accretion disc model. These models have basically two input parameters, the mass of the central black hole and the accretion rate. We use the model first proposed by Shakura & Sunyaev (1973), which involves a geometrically thin, optically thick steady accretion disc (Pringle 1981; Czerny & Elvis 1987). The disc spectrum is the following:

$$L_{\nu,th} = \pi \int_{fR_G}^{R_{out}} \frac{2h\nu^3}{c^2} \frac{2\pi R dR}{e^{h\nu/KT_S(R)} - 1}, \quad (1)$$

where $R_G = GM/c^2$ is the gravitational radius, fR_G is the radius of the innermost stable orbit and R_{out} is the maximum distance from the central black hole at which the spectrum is computed. Finally, $T_S(R)$ is the surface temperature of the accretion disc and is given by:

$$T_S(R) = \left[\frac{3GM\dot{M}}{8\pi R^3\sigma} \left(1 - \left(\frac{R_G}{R} \right)^{1/2} \right) \right]^{1/4}, \quad (2)$$

where σ is the Stefan constant and M and \dot{M} are the mass of the central black hole and the accretion rate, respectively.

In principle, one can evaluate M using the formula

$$M = \frac{V^2 R}{aG}, \quad (3)$$

once the distance R and the velocity V of a body in the gravitational field of the black hole are known. Here $a = 2$ for a body in free-fall and $a = 1$ for an orbiting body. While the velocity of the gas in the BLR can be evaluated quite easily from observed spectra using the line widths, the determination of the distance R is not straightforward. Basically, two different methods can be used (see Wandel, Peterson & Malkan 1999). The first one is indirect and relies on photoionization theory (e.g., Netzer 1990) by using the definition of the ionization parameter U (proportional to the flux of ionizing photons per electron):

$$U = \frac{Q}{4\pi R^2 n_e c}, \quad (4)$$

where

$$Q = \int_{13.6\text{eV}}^{\infty} \frac{L_\nu}{h\nu} d\nu \quad (5)$$

is the number of ionizing photons per unit of time and n_e is the electronic density in the shell of the BLR at distance R from the center. The second method, more direct, takes advantage of the reverberation-mapping technique (e.g., Peterson 1993). This allows one to evaluate the radius of the

BLR by measuring the time lags between variations in the broad emission lines and the ionizing continuum.

We can see that in order to evaluate R from eq. (4) we need to know $U n_e$ and Q . The latter has been calculated as follows. We assume for our sources an average optical to X-ray effective spectral index $\alpha_{\text{ox}} = 1.56$, equal to that measured by Laor et al. (1997) for the 19 radio-quiet quasars from the Bright Quasar Survey. We then substitute in eq. (5) $L_\nu = L_{13.6}(\nu/\nu_{13.6})^{-\alpha_{\text{ox}}}$ and calculate $L_{13.6}$ for every single object using the equation:

$$L_{\text{ion}} = f_{\text{cov}}^{-1} L_{\text{BLR}} = \int_{13.6 \text{ eV}}^{\infty} L_\nu d\nu, \quad (6)$$

where L_{ion} is the power of the ionizing continuum and f_{cov} is the BLR covering factor, which we assume to be ~ 10 per cent (see next subsection).

The second quantity needed, $U n_e$, varies from line to line, due to the complex structure of the BLR. This parameter can be estimated from eq. (4) if the distance of the clouds emitting a particular line is known. This is available for a sizeable sample of source for $H\beta$ (e.g., Wandel et al. 1999 and references therein) since this line is easy to observe in low-redshift, and better studied, AGN. By comparing the radius measured with the reverberation mapping techniques with that evaluated with the photoionization model for 18 sources we derive $(U n_e)_{H\beta} \sim 5 \times 10^9 \text{ cm}^{-3}$. However, our sample has an average redshift $z \sim 1.5$, which means that only a relatively small number of sources (32) has $H\beta$ information. We then need an estimate of $U n_e$ for some lines in the UV band, which unfortunately have not been studied exhaustively yet. Fromerth and Melia (2000) have recently published the distances of the C IV line region for five AGN, evaluated using the reverberation mapping technique. We can then use these values and the $H\beta$ distances for the same objects (Wandel et al. 1999) to evaluate $(U n_e)_{\text{CIV}}$ as follows:

$$(U n_e)_{\text{CIV}} = (U n_e)_{H\beta} \left(\frac{R_{H\beta}}{R_{\text{CIV}}} \right)^2. \quad (7)$$

We perform this calculation for all the five objects and we then compute an average to obtain $(U n_e)_{\text{CIV}} = 1.34 \times (U n_e)_{H\beta} \sim 6.7 \times 10^9 \text{ cm}^{-3}$. With this value we can evaluate R_{CIV} for 40 more objects (the ones showing the C IV line).

From the full width half maximum (FWHM) values and from eq. (3) we calculate the masses for these 72 objects, using $a = 1$ and $V = 1.5$ FWHM, which represents a reasonable choice for radio-loud quasars, as suggested by McLure and Dunlop (2001). In a handful of cases (and only for $H\beta$) we found a relatively strong narrow component associated with the line which, if not subtracted, would have given a spuriously low value for the FWHM (and therefore the mass). In those cases the FWHM values we are using refer to the broad component of the lines. The relation between the derived mass and the ionizing power L_{ion} is plotted in Figure 1. We find a very strong correlation ($P \sim 99.99$ per cent) between the two quantities, with $M \propto L_{\text{ion}}^{0.43 \pm 0.06}$, and then use this correlation to evaluate the masses for the 64 FSRQ without $H\beta$ or C IV information. Note that such a dependence is not unexpected: in our sample we find no cor-

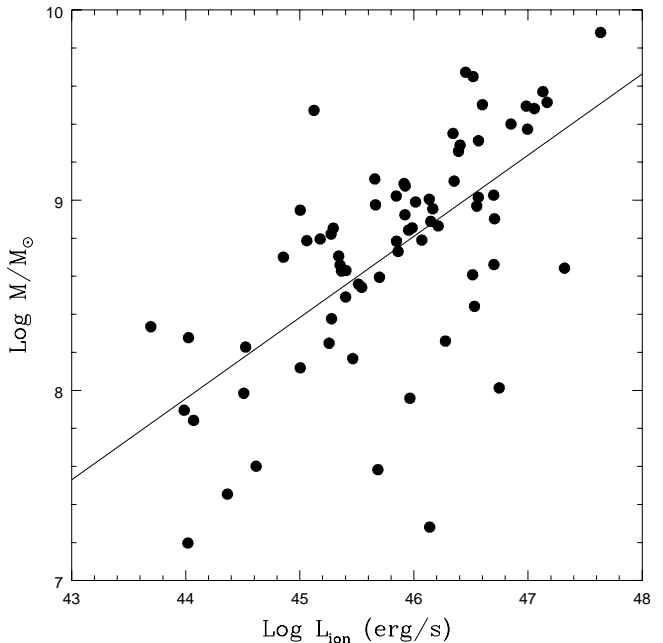


Figure 1. The mass-ionizing power relation for the 72 FSRQ having $H\beta$ or C IV line in their spectra. The solid line is the best fit to the data: $\log(M/M_\odot) = 0.43 \log L_{\text{ion}} - 10.8$.

relation between FWHM and L_{ion} and therefore, since we assume $R_{\text{BLR}} \propto Q^{0.5} \propto L^{0.5}$, we will obtain $M \propto L_{\text{ion}}^{0.5}$.

The second parameter needed to compute any accretion disc model is the accretion rate of mass onto the central black hole (\dot{M}). This quantity is calculated using the following relation:

$$L_{\text{ion}} = \epsilon \dot{M} c^2, \quad (8)$$

where ϵ is the efficiency parameter. In the following we assume that the black holes in the center of our FSRQ are rapidly rotating, so that we choose $\epsilon \sim 0.3$ (Malkan 1982).

We finally evaluate the Eddington ratio for all the 136 sources for which mass and accretion rate have been calculated:

$$\frac{L}{L_{\text{Edd}}} = 4.5 \epsilon \frac{\dot{M}}{M_8}, \quad (9)$$

where \dot{M} is expressed in M_\odot/yr and $M_8 = 10^8 M_\odot$. Table 1 gives masses, accretion rates, and Eddington ratios for all our FSRQ. Note that masses span the range $2 \times 10^7 - 7 \times 10^9 M_\odot$, with $\langle \log M \rangle = 8.74 \pm 0.04 M_\odot$, while accretion rates cover the range $3 \times 10^{-3} - 72 M_\odot/\text{yr}$, with $\langle \log \dot{M} \rangle = -0.40 \pm 0.07 M_\odot/\text{yr}$.

Figure 2 shows the distribution of the Eddington ratio, which lies between 0.002 and 1 for almost all the FSRQ, with $\langle \log L/L_{\text{Edd}} \rangle = -1.02 \pm 0.05$. Only four sources ($\sim 3\%$) have $L/L_{\text{Edd}} > 1$, which is reassuring. The average value for the 32 $H\beta$ sources is $10^{-1.3 \pm 0.1}$, that for the 40 C IV ones is $10^{-0.81 \pm 0.09}$ and the one for the remaining 64 sources is $10^{-1.0 \pm 0.1}$.

Note that by using eq. (4) we assume that $R_{\text{BLR}} \propto$

Table 1. Masses, Accretion Rates, Eddington Ratios and Luminosities

Name	$\log M$ M_{\odot}	$\log \dot{M}$ M_{\odot}/yr	$\log L/L_{Edd}$	$\log L_{th}/L_{tot}^{(1)}$	$\log L_{tot}^{(1)}$ $erg\ s^{-1}\ Hz^{-1}$	$\log L_{th}/L_{tot}^{(2)}$	$\log L_{tot}^{(2)}$ $erg\ s^{-1}\ Hz^{-1}$	$\log L_{th}/L_{tot}^{(3)}$	$\log L_{tot}^{(3)}$ $erg\ s^{-1}\ Hz^{-1}$
WGAJ0010.5–3027 ^c	8.8	-0.3	-0.9	-1.0	30.89
WGAJ0010.7–3649 ^b	9.3	0.2	-1.0	-1.6	32.04	-1.4	31.78
WGAJ0011.2–3620 ^b	8.8	-0.3	-1.0	-0.4	30.28
WGAJ0012.5–1629 ^a	7.2	-2.2	-1.3	-1.5	28.98
WGAJ0014.5–3059 ^b	9.5	0.4	-1.0	-1.0	31.66
WGAJ0029.0+0509 ^b	9.4	0.1	-1.1	-0.9	31.31
WGAJ0032.5–2648 ^c	8.9	0.1	-0.8	-0.4	30.58
WGAJ0049.5–2509 ^b	7.5	-1.9	-1.2
PKS 0100–270 ^b	8.9	-0.2	-1.0
WGAJ0106.7–1034 ^a	8.7	-0.9	-1.4	-0.7	30.02
WGAJ0110.5–1647 ^c	8.9	-0.1	-0.8	-0.8	30.82	-0.8	30.88
1Jy0112–017 ^b	9.0	-0.6	-1.4
1Jy0119+041 ^c	8.6	-0.6	-1.1
UM 320 ^b	8.9	-0.1	-0.9
WGAJ0126.2–0500 ^a	8.2	-1.7	-1.8	-0.9	29.34
WGAJ0136.0–4044 ^c	8.3	-1.5	-1.6	-1.2	29.79
WGAJ0143.2–6813 ^c	8.6	-0.8	-1.3	-0.7	30.02
WGAJ0146.2+0223 ^b	8.3	0.0	-0.1	-1.6	31.39	-1.5	31.28
WGAJ0210.0–1004 ^b	9.0	-0.4	-1.3	-1.0	30.93	-0.9	30.75
WGAJ0210.1–3851 ^b	9.5	0.8	-0.5	-0.6	31.68
WGAJ0216.6–7331 ^b	9.0	0.5	-0.4	-0.8	31.30
WGAJ0217.7–7347 ^c	8.7	-0.4	-1.0	-0.7	30.43
WGAJ0227.5–0847 ^b	9.6	0.9	-0.6	-0.5	31.67	-0.4	31.52
PKS 0256–005 ^c	8.9	-1.2	-2.1	-0.3	29.55
WGAJ0258.6–5052 ^c	9.2	0.8	-0.4
WGAJ0259.4+1926 ^a	8.2	-1.7	-1.7	-1.9	30.35
WGAJ0304.9+0002 ^a	8.5	-0.8	-1.2	-0.7	29.92	-0.6	29.92
WGAJ0312.3–6610 ^c	8.5	-1.0	-1.4	-1.0	30.18
WGAJ0314.4–6548 ^a	8.7	-0.9	-1.5	-0.5	29.84
WGAJ0322.1–5205 ^a	8.9	-0.9	-1.7	-0.7	30.11
WGAJ0322.2–5042 ^a	8.6	-0.9	-1.4	-0.5	29.81
WGAJ0322.6–1335 ^b	8.8	-1.0	-1.7	-0.3	29.61	-0.3	29.70
WGAJ0324.9–2140 ^b	9.9	1.4	-0.4	-0.4	32.07	-0.3	32.01
WGAJ0357.6–4158 ^c	8.7	-0.5	-1.1	-0.6	30.24
WGAJ0411.0–1637 ^a	9.1	0.1	-0.9	0.0	30.31
WGAJ0424.6–3849 ^b	8.0	-0.3	-0.1	-0.6	29.98	-0.4	29.82
WGAJ0427.2–0756 ^b	9.7	0.2	-1.3	0.2	30.50
WGAJ0434.3–1443 ^b	9.1	-0.3	-1.3	-1.5	31.45	-1.0	30.93
WGAJ0435.1–0811 ^a	7.6	-0.5	0.0	-1.0	29.83	-1.0	29.92
WGAJ0441.8–4306 ^c	8.1	-1.8	-1.8	-1.2	29.48	-0.6	28.98
WGAJ0447.9–0322 ^c	9.2	0.6	-0.5	-0.7	31.31	-0.7	31.38
WGAJ0448.2–2110 ^b	8.7	0.5	-0.1	-1.2	31.50	-0.8	31.11
WGAJ0448.6–2203 ^c	8.0	-2.2	-2.1	-0.5	28.46
WGAJ0510.0+1800 ^c	8.2	-1.6	-1.7	-1.8	30.29
1Jy0514–459 ^a	7.6	-1.6	-1.1
WGAJ0535.1–0239 ^c	8.9	0.1	-0.8	-0.5	30.67	-0.4	30.60
WGAJ0539.0–3427 ^a	8.3	-2.5	-2.8	-0.4	28.32
WGAJ0546.6–6415 ^a	9.1	-0.3	-1.3	-0.5	30.50
WGAJ0600.5–3937 ^c	8.9	0.0	-0.8	-1.0	31.14	-0.9	31.11
WGAJ0631.9–5404 ^a	9.5	-1.1	-2.5	-0.2	29.74
WGAJ0648.2–4347 ^c	9.0	0.1	-0.7	-0.9	31.06	-0.7	30.94
S5 0743+74 ^c	8.9	0.0	-0.8	-1.6	31.71	-1.3	31.47
WGAJ0744.8+2920 ^c	8.8	-0.2	-0.9
WGAJ0747.0–6744 ^c	8.6	-0.8	-1.3	-0.4	29.74
WGAJ0748.2–5257 ^b	9.3	0.3	-0.9	-0.8	31.36	-0.7	31.30
WGAJ0751.0–6726 ^c	8.9	0.0	-0.8	-0.7	30.77	-0.7	30.86
1Jy0850+581 ^c	9.3	0.8	-0.3
OJ–297 ^c	9.1	0.5	-0.5
1Jy0859+470 ^b	8.0	0.5	0.6
WGAJ0927.7–0900 ^a	7.8	-2.2	-1.9	-1.1	28.96
WGAJ0937.2+5008 ^a	8.3	-2.2	-2.4	-1.5	29.65
WGAJ1003.9+3244 ^b	9.3	0.2	-1.0	-0.3	30.73
WGAJ1006.5+0509 ^c	8.5	-0.9	-1.3	0.1	29.16
WGAJ1010.8–0201 ^a	8.8	-0.4	-1.0	-0.7	30.40	-0.5	30.27
WGAJ1011.5–0423 ^c	9.0	0.1	-0.7	-0.9	31.08	-0.7	30.96
WGAJ1025.9+1253 ^a	9.3	0.8	-0.3	0.4	30.42
WGAJ1026.4+6746 ^c	8.2	-1.0	-1.1	-1.0	29.97
S5 1027+74 ^a	8.1	-1.9	-1.9	-1.8	30.07	-1.1	29.41
WGAJ1028.5–0236 ^c	7.9	-2.2	-2.0
WGAJ1032.1–1400 ^c	8.7	-0.4	-1.0	-0.9	30.56	-0.7	30.41
WGAJ1035.0+5652 ^c	8.3	-1.4	-1.6	-0.9	29.59
WGAJ1046.3+5354 ^b	9.0	0.3	-0.5	-0.5	30.92
B2 1048+34 ^c	9.1	0.5	-0.5
WGAJ1101.8+6241 ^a	8.2	-0.8	-0.8	-0.8	29.82
WGAJ1104.8+6038 ^c	9.0	0.3	-0.6	-0.4	30.75
WGAJ1105.3–1813 ^a	8.4	-1.0	-1.2	-0.7	29.73	-0.6	29.72
WGAJ1112.5–3745 ^c	8.8	-0.2	-0.9	-0.8	30.67	-0.6	30.51

Table 1. (Continued)

Name	$\log M$ M_{\odot}	$\log \dot{M}$ M_{\odot}/yr	$\log L/L_{Edd}$	$\log L_{th}/L_{tot}^{(1)}$	$\log L_{tot}^{(1)}$ $\text{erg s}^{-1} \text{Hz}^{-1}$	$\log L_{th}/L_{tot}^{(2)}$	$\log L_{tot}^{(2)}$ $\text{erg s}^{-1} \text{Hz}^{-1}$	$\log L_{th}/L_{tot}^{(3)}$	$\log L_{tot}^{(3)}$ $\text{erg s}^{-1} \text{Hz}^{-1}$
WG AJ1116.1+0828 ^c	8.0	-2.0	-2.0	-1.8	29.89
WG AJ1150.4+0156 ^c	9.0	0.2	-0.7	-0.2	30.57
WG AJ1206.2+2823 ^c	8.6	-0.8	-1.3	-0.6	29.87	-0.4	29.70
WG AJ1213.2+1443 ^c	8.7	-0.6	-1.1	-0.3	29.75
WG AJ1217.1+2925 ^c	8.5	-1.0	-1.3	-0.3	29.47
WG AJ1223.9+0650 ^c	8.6	-0.6	-1.2	-0.6	30.15
WG AJ1300.7-3253 ^c	8.8	-0.2	-0.9	-1.0	30.45
WG AJ1314.0-3304 ^c	8.5	-0.9	-1.3	-0.5	29.70
WG AJ1315.1+2841 ^c	8.9	0.0	-0.8	-0.9	30.97
WG AJ1324.0-3623 ^a	8.8	-0.2	-0.8	-0.9	30.77	-0.7	30.67
WG AJ1333.1-3323 ^b	9.0	-0.2	-1.1	-0.6	30.57	-0.5	30.49
WG AJ1337.2-1319 ^b	9.4	0.8	-0.5	-1.1	32.07	-1.0	31.99
WG AJ1359.6+4010 ^a	8.0	-1.7	-1.6	-1.7	30.03
WG AJ1400.7+0425 ^b	8.6	-0.5	-1.0	-1.2	30.83
WG AJ1402.7-3334 ^b	8.8	-1.1	-1.7	-1.7	30.99	-1.3	30.58
WG AJ1406.9+3433 ^b	9.5	0.9	-0.5	-0.8	31.95	-0.5	31.67
WG AJ1416.4+1242 ^a	8.8	-1.2	-1.8	-0.4	29.53
WG AJ1417.5+2645 ^b	8.6	-0.8	-1.3	-0.7	30.06
WG AJ1419.1+0603 ^b	9.0	-0.1	-0.9	-0.6	30.73	-0.6	30.73
WG AJ1442.3+5236 ^c	9.0	0.3	-0.6	-0.8	31.27
WG AJ1457.7-2818 ^b	9.7	0.3	-1.2	-0.5	31.22	-0.5	31.14
1Jy1502+106 ^c	9.0	0.3	-0.6
WG AJ1506.6-4008 ^c	8.9	0.0	-0.8	-0.7	30.73	-0.6	30.73
WG AJ1509.5-4340 ^a	8.7	-0.4	-1.0	-0.6	30.28	-0.7	30.41
WG AJ1525.3+4201 ^c	8.9	0.0	-0.8	-0.9	30.96
WG AJ1543.6+1847 ^c	8.8	-0.2	-0.9	-0.5	30.46
WG AJ1610.3-3958 ^a	8.1	-1.2	-1.2	-1.7	30.46
OS319 ^b	9.4	0.6	-0.7
WG AJ1615.2-0540 ^b	8.9	-0.3	-1.1	-2.6	32.55
WG AJ1629.7+2117 ^c	8.4	-1.1	-1.4
4C38.41 ^b	8.6	1.1	0.6
1Jy1637+574 ^a	8.4	0.3	0.0
1Jy1638+398 ^c	8.5	-0.9	-1.3
3C345 ^a	8.9	0.5	-0.3
WG AJ1656.6+5321 ^c	8.9	-0.1	-0.8	-0.3	30.33
WG AJ1656.6+6012 ^a	8.5	-0.7	-1.1	-0.7	30.07
1Jy1725+044 ^c	8.6	-0.8	-1.2
WG AJ1738.6-5333 ^b	9.5	0.8	-0.6	-1.1	32.07	-0.8	31.76
WG AJ1804.7+1755 ^a	8.6	-0.7	-1.2	-0.7	30.08
WG AJ1808.2-5011 ^b	8.9	0.0	-0.8	-0.8	30.86
WG AJ1826.1-3650 ^c	8.6	-0.8	-1.3	-1.4	30.70	-1.1	30.40
WG AJ1827.1-4533 ^c	9.0	0.2	-0.7	-0.7	31.04
WG AJ1837.7-5848 ^b	9.0	0.3	-0.6	-1.0	31.45
WG AJ1911.8-2102 ^c	8.8	-0.3	-1.0	-1.0	30.76
PKS 1937-101 ^c	9.7	1.9	0.3
PKS 2059+034 ^c	8.9	0.0	-0.8
WG AJ2109.7-1332 ^c	9.1	0.4	-0.5	-0.8	31.32	-0.7	31.21
WG AJ2154.1-1502 ^c	9.2	0.8	-0.4	-0.7	31.47	-0.6	31.41
WG AJ2157.7+0650 ^a	8.7	-1.4	-2.0	-0.7	29.67	0.0	29.02
WG AJ2159.3-1500 ^b	8.6	0.3	-0.2	-1.5	31.65	-1.3	31.51
OY-106 ^c	8.4	-1.1	-1.4
WG AJ2248.6-2702 ^b	9.1	-0.6	-1.6	-1.9	31.73	-1.4	31.18
WG AJ2320.6+0032 ^b	9.0	-0.1	-1.0	-1.5	31.56	-0.9	30.97
WG AJ2322.0+2113 ^a	7.3	-0.1	0.7	-0.6	30.55	-0.6	30.66
WG AJ2329.0+0834 ^c	8.4	-1.2	-1.5	-0.8	29.69
WG AJ2333.2-0131 ^c	8.7	-0.6	-1.1	-0.3	29.86
1Jy2344+092 ^c	9.1	0.5	-0.5
WG AJ2349.9-2552 ^c	8.7	-0.5	-1.1	-0.9	30.40	-0.5	30.10
WG AJ2354.2-0957 ^c	8.3	-1.5	-1.7	-1.5	30.13

(1) Values calculated in the interval $7.08 \times 10^{14} - 7.24 \times 10^{14}$ Hz.

(2) Values calculated in the interval $1.32 \times 10^{15} - 1.35 \times 10^{15}$ Hz.

(3) Values calculated in the interval $2.24 \times 10^{15} - 2.29 \times 10^{15}$ Hz.

^a Sources whose mass has been calculated using the $H\beta$ line.

^b Sources whose mass has been calculated using the C IV line.

^c Sources whose mass has been calculated using the correlation luminosity-mass (see Fig. 1).

$Q^{0.5} \propto L^{0.5}$. This is in apparent contrast with Kaspi et al. (2000), who found $R_{BLR} \propto L^{0.70 \pm 0.03}$. However, Vestergaard (2002), by properly taking into account measurement uncertainties in both R_{BLR} and L , has obtained a flatter dependency with a slope of 0.58 ± 0.09 , fully consistent with our assumption.

Recently, Vestergaard (2002) has also derived a relationship to estimate AGN masses based on UV luminosity

and the FWHM of C IV. This was calibrated on recent estimates of low-redshift AGN masses obtained via reverberation mapping using the $H\beta$ line. A comparison between our mass estimates for the 40 objects with C IV data in our sample and those derived using Vestergaard's relationship shows that the two are in extremely good agreement, with a basically linear dependence (1.16 ± 0.04). The means for the two methods are 8.99 ± 0.08 and 8.98 ± 0.09 respectively, and

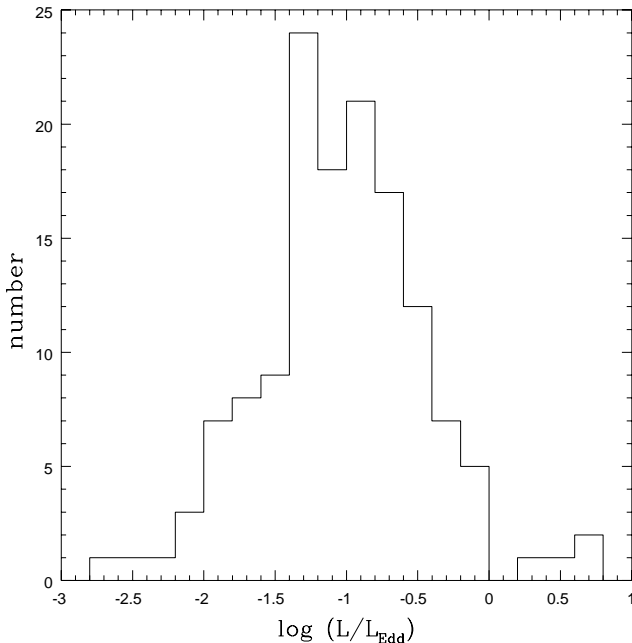


Figure 2. The distribution of the Eddington ratio L/L_{Edd} for our FSRQ.

the two distributions are not significantly different according to a Kolmogorov-Smirnov (KS) test.

3.1 Covering Factor

The covering factor of the BLR in (mostly radio-quiet) AGN has been discussed by several authors in the past (see Maiolino et al. 2001 and references therein). Early estimates of this quantity seemed to indicate a covering factor $f_{cov} \sim 5 - 10$ per cent, while recent observations indicate instead $f_{cov} \sim 30$ per cent. Estimates of the covering factor need measurements of the UV continuum emission from the accretion disc. In the case of blazars this emission is swamped by the jet and this makes the covering factor a difficult quantity to calculate for these sources. The only way to get a rough estimate of f_{cov} is to know the luminosity of the BLR of objects in which the thermal emission is clearly dominating the synchrotron one. We find in literature only two of these objects: 3C 273 and PKS 2149–306. For the first source (see Kriss et al. 1999 and Celotti et al. 1997 for the data) we estimate $f_{cov} \sim 7$ per cent, while for the second one (Elvis et al. 2000; Wilkes et al. 1983) we find $f_{cov} \sim 10$ per cent. For this reason, we adopt $f_{cov} \sim 10$ per cent for our sources and we comment on how our results would change with $f_{cov} = 30$ per cent.

4 TESTING THE METHOD

Before computing the thermal contribution for our FSRQ sample, we need to know if our method is reliable. The best way to do this is to evaluate masses and accretion rates for a sample of radio-quiet quasars (which are not affected by beaming), compute their thermal emission, and compare

it with the data. All we need to know for such a test is the power of the BLR, the effective spectral index α_{ox} , the FWHM of $H\beta$ or C IV and a measure of the luminosity in the optical-UV band. Laor et al. (1997) give for 19 low-redshift radio-quiet quasars the luminosity at 10^{15} Hz, α_{ox} , and the FWHM and power of $H\beta$ (see their Table 4; we excluded the 4 radio-loud quasars in their list). The only missing parameter is L_{BLR} , but we can estimate it assuming $L_{H\beta} / L_{BLR} \sim 0.04$ (Francis et al. 1991; Celotti et al. 1997).

We use eq. (3) to evaluate the masses and eq. (8) with $\epsilon = 0.057$ (assuming non-rotating black holes, see Misner, Thorne & Wheeler 1970) to evaluate the accretion rates; we then compute the accretion disc spectra using eq. (1) with $f = 6$, because in non-rotating black holes (which is likely the case in radio-quiet sources; e.g., Wilson & Colbert 1995; Moderski, Sikora & Lasota 1998) the main stable orbit is roughly located at six times the gravitational radius.

To perform a realistic comparison between the data and our model we take into account the fact that in radio-quiet quasar spectra the thermal contribution emerges from a power law (see Malkan 1982; Band & Malkan 1989) and thus it is dominant only around its peak. For this reason, we extrapolate the observed luminosity at the frequency of the maximum of the computed thermal emission, using for each source its α_{ox} .

In Table 2 we give, for each of the 19 sources, the computed thermal luminosity, the extrapolated luminosity from the data at the peak frequency (ν_P) of the thermal emission and the ratio between the two powers.

The average logarithmic ratio is -0.35 ± 0.05 ; this means that the observed luminosity is, on average, ~ 50 per cent smaller than that computed with the accretion disc model. If we use $f_{cov} = 30$ per cent, which should represent the optimal choice for radio-quiet AGN as discussed in Section 3.1, the average logarithmic ratio modifies to 0.13 ± 0.05 . That is, the observed luminosity is, on average, ~ 35 per cent larger than that from the accretion disc model. Given the many assumptions involved in our model this agreement is quite remarkable.

Before evaluating the thermal power of our objects we comment on how our results depend on the mass estimates. For example, an increase of a factor 2 in the black hole mass will result in an increase of a factor $\sim 2^{1/2}$ of the power at the peak of the thermal emission, but the frequency of such peak will be lowered by roughly the same factor. The total thermal power does not depend on the mass, because it is basically given by $\epsilon \dot{M} c^2 = L_{ion}$.

5 DISENTANGLING THE LUMINOSITY COMPONENTS

The results reported in the previous section suggest that the method we are using to evaluate the thermal emission from the accretion disc in FSRQ is quite reliable.

We then use the previously evaluated masses and accretion rates to compute the accretion disc spectra. This time we choose $f = 1.23$ in eq. (1), a value more appropriate for rotating black holes (Malkan 1982), a situation appropriate for radio-loud sources (e.g., Wilson & Colbert 1995; Moderski, Sikora & Lasota 1998). The thermal spectra have been computed for all the 136 sources, but optical spectra

Table 2. Masses, Accretion Rates and Luminosities for Bright Quasar Survey Sources

Name (PG)	M_8	\dot{M} (M_\odot/yr)	ν_P (Hz)	$L_{th}(\nu_P)$ ($\text{erg s}^{-1} \text{ Hz}^{-1}$)	$L_{ext}(\nu_P)$ ($\text{erg s}^{-1} \text{ Hz}^{-1}$)	$\log(L_{ext}/L_{th})$
0947+396	14	1.8	1.2×10^{15}	2.0×10^{30}	1.3×10^{30}	-0.200
0953+414	14	10	1.8×10^{15}	7.3×10^{30}	3.1×10^{30}	-0.372
1001+054	1.0	1.4	4.2×10^{15}	4.4×10^{29}	5.4×10^{28}	-0.911
1048+342	11	3.3	1.6×10^{15}	2.7×10^{30}	6.9×10^{29}	-0.598
1114+445	12	1.6	1.3×10^{15}	1.6×10^{30}	8.2×10^{29}	-0.294
1115+407	1.1	0.66	3.3×10^{15}	2.6×10^{29}	1.5×10^{29}	-0.233
1116+215	13	11	2.0×10^{15}	7.3×10^{30}	2.5×10^{30}	-0.457
1202+281	14	1.5	1.1×10^{15}	1.7×10^{30}	8.9×10^{29}	-0.286
1216+069	39	10	1.1×10^{15}	1.2×10^{31}	7.6×10^{30}	-0.205
1322+659	4.0	1.3	2.1×10^{15}	8.1×10^{29}	7.2×10^{29}	-0.051
1352+183	9.0	2.8	1.7×10^{15}	2.2×10^{30}	8.4×10^{29}	-0.417
1402+261	2.2	1.8	3.0×10^{15}	7.8×10^{29}	5.4×10^{29}	-0.164
1411+442	3.6	1.2	2.2×10^{15}	7.2×10^{29}	1.6×10^{29}	-0.645
1415+451	2.2	0.51	2.2×10^{15}	3.0×10^{29}	1.9×10^{29}	-0.201
1427+480	4.3	2.1	2.5×10^{15}	1.6×10^{30}	4.4×10^{29}	-0.552
1440+356	0.77	0.66	4.0×10^{15}	2.1×10^{29}	1.1×10^{29}	-0.310
1444+407	4.6	2.5	2.3×10^{15}	1.4×10^{30}	1.1×10^{30}	-0.101
1543+489	2.4	4.8	3.7×10^{15}	1.7×10^{30}	6.9×10^{29}	-0.383
1626+554	11	1.5	1.3×10^{15}	1.5×10^{30}	7.3×10^{29}	-0.320

are only available for the 113 objects newly identified by the DXRBS. For this reason, the remaining 24 FSRQ have not been used in the following analysis.

The λ vs. f_λ measured optical spectra were converted to ν vs. L_ν using our adopted cosmology and were k-corrected using the optical spectral indices α_{opt} from the DXRBS database. The computed thermal spectra were then compared to the observed ones.

An interesting quantity to measure is the ratio of thermal to total power at a fixed rest-frame frequency. Unfortunately, the spread in redshift of the sources makes it impossible to evaluate this ratio at the same frequency for all objects. We then selected three rest-frame frequency intervals around the line-free continuum zones discussed by Forster et al. (2001) to evaluate the ratio L_{th}/L_{tot} in these bands for the FSRQ sample. Namely, the interval $7.08 \times 10^{14} - 7.24 \times 10^{14}$ Hz is covered by 54 objects, the $1.32 \times 10^{15} - 1.35 \times 10^{15}$ Hz one is covered by 76 sources, while 27 spectra cover the interval $2.24 \times 10^{15} - 2.29 \times 10^{15}$ Hz. L_{th} was evaluated at the central frequency of the interval, while L_{tot} was obtained by taking the mean power in the interval. In cases where the frequency interval fell into the noise or included strong absorption lines the ratio was not determined.

Table 1 reports the ratio L_{th}/L_{tot} and L_{tot} for the three frequency bands for the individual sources. Table 3 gives mean and median values for $\log L_{th}/L_{tot}$ for all three bands, the percentage of objects with $L_{th}/L_{tot} < 0.5$ (i.e., thermal to non-thermal power ratio < 1) per band, and the mean redshift of the sources. Note that for some sources two of the selected intervals fall within the observed spectrum so two ratios are available. Fig. 3 shows the distribution of $\log L_{th}/L_{tot}$ in the three bands.

Table 3 and Fig. 3 show that, typically, the non-thermal component dominates, as the thermal one makes up ~ 15 per cent of the optical/UV power. Moreover, $\gtrsim 91$ per cent of the L_{th}/L_{tot} values are below 0.5, which means that in only $\lesssim 9$ per cent of the cases the thermal power is larger than the non-thermal one. Note that L_{th}/L_{tot} is > 1 , an

unphysical result, only in 3 cases ($\sim 2 - 3$ per cent). This is another confirmation of the reliability of our method.

The spectra of the majority (~ 70 per cent) of our FSRQ have not been observed at parallactic angle, which results in a flux loss due to atmospheric differential refraction, more pronounced in the blue part of the spectrum. We have nevertheless included all the sources in our study, based on three facts: 1. the loss at the position of a given line, as tabulated by Filippenko (1982), is $\gtrsim 30$ per cent only in ~ 10 per cent of the cases; this is due to the fact that most observations were done with the source at meridian; 2. the L_{th}/L_{tot} ratio for sources observed at parallactic angle is not significantly different from that for sources not observed at parallactic angle. In particular, in the $1.32 \times 10^{15} - 1.35 \times 10^{15}$ Hz range, which is the most populated one, L_{th}/L_{tot} for the parallactic angle sources is ~ 30 per cent smaller than for all sources; if anything, then, this would go in the direction of decreasing the thermal component; 3. the parameter which enters more prominently in our calculations is L_{BLR} , which is in most cases based on more than one line. The effect of the parallactic angle, therefore, gets diluted. Slit sizes during our observations were matched to the seeing. We are not aware of any other systematic effects which could have influenced our flux calibration.

We now use the luminosity values to perform correlations between powers. Two possible complications should be kept in mind: first, when correlating luminosities one has to be particularly careful to remove the (generally) common redshift dependence which can introduce spurious correlations. The proper way of dealing with the problem is to examine the correlations between luminosities excluding the dependence on redshift, i.e., via a partial correlation analysis (see Kendall & Stuart 1979; Anderson 1984); second, the three frequency ranges sample different redshifts, as shown in Tab. 3, and therefore the comparison is subject to possible evolutionary effects.

We have correlated the thermal power L_{th} with the non-thermal one, L_{nt} , starting from the $1.32 \times 10^{15} - 1.35 \times 10^{15}$ Hz range, which includes the largest number of sources. We

Table 3. Thermal to Total Power Ratios

Band	$\log L_{th}/L_{tot}$		N	Percentage < 0.5	Mean redshift
	Mean	Median			
$(7.08 - 7.24) \times 10^{14}$ Hz	-0.85 ± 0.07	-0.73	54	91	0.67 ± 0.04
$(1.32 - 1.35) \times 10^{15}$ Hz	-0.75 ± 0.05	-0.70	76	93	1.43 ± 0.07
$(2.24 - 2.29) \times 10^{15}$ Hz	-0.92 ± 0.09	-0.85	27	100	2.32 ± 0.10

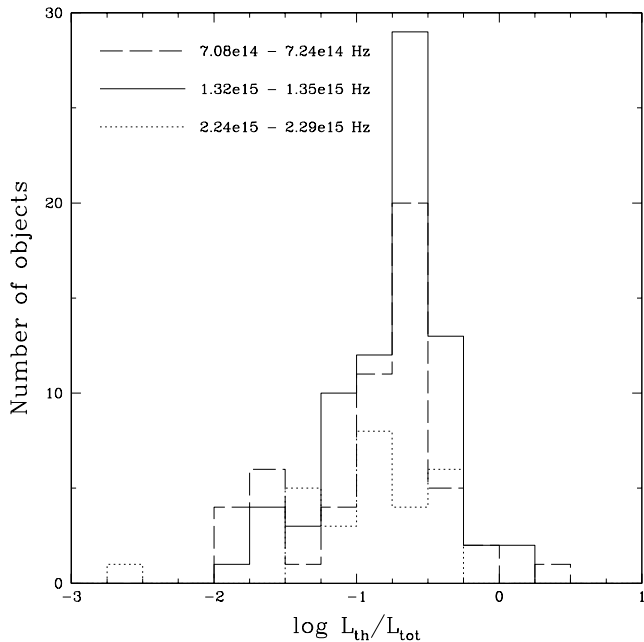


Figure 3. The distribution of the ratios of thermal to total luminosity in three line-free continuum intervals: $7.08 \times 10^{14} - 7.24 \times 10^{14}$ Hz (dashed line), $1.32 \times 10^{15} - 1.35 \times 10^{15}$ Hz (solid line), $2.24 \times 10^{15} - 2.29 \times 10^{15}$ Hz (dotted line).

assume that two components make up the optical/UV emission in our sources, a thermal one related to the accretion disc, and a non-thermal one related to the jet. The former has then been derived by subtracting the thermal from the total power, i.e., $L_{nt} = L_{tot} - L_{th}$. Fig. 4 shows that the two quantities are strongly correlated ($P > 99.99$ per cent, $R = 0.80$). This is true even when the common redshift dependence is subtracted off. Note that the observed strong correlation cannot be due to the fact that the two powers are not strictly independent, as that would result in an *anti-correlation* between the two quantities. Both powers are also strongly correlated with optical power L_o (defined at 5,000 Å) but, again, their mutual correlation remains highly significant ($P > 99.9$ per cent) even when this common dependence is taken into account. (We note that the $L_{nt} - L_o$ correlation is expected, given that $L_{nt} \approx L_o$.) The fact that $L_{th} \propto L_{nt}^{0.62 \pm 0.05}$ suggests that the L_{th}/L_{tot} ratio depends on luminosity. Indeed, we find a strong anti-correlation between L_{th}/L_{tot} and L_{nt} (but not L_{th}), i.e., the stronger the non-thermal power, the lower the thermal fraction, with this ratio approaching unity at the low end of our luminosity range (see Fig. 4). This could indicate that only in less powerful (possibly less beamed?) sources the thermal component

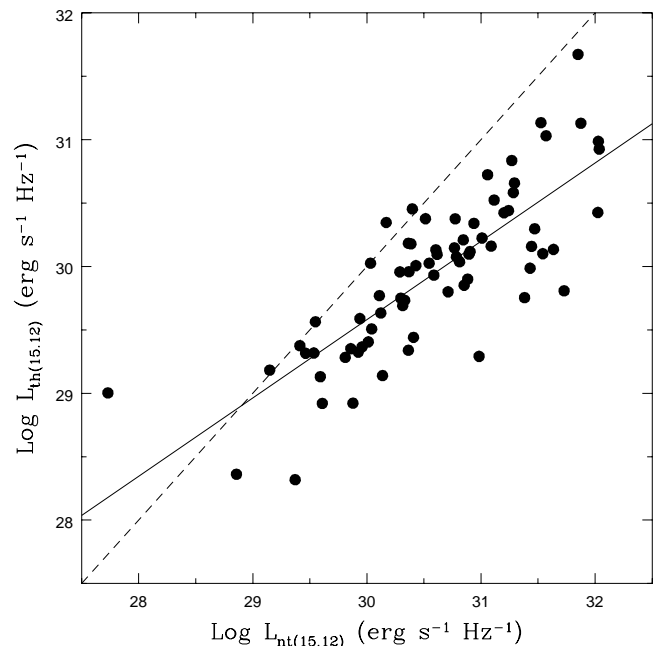


Figure 4. The thermal vs. non-thermal luminosity relation at $\log \nu = 15.12$ Hz (rest-frame) for our FSRQ. The solid line is our best fit to the data: $\log L_{th} = 0.62 \log L_{nt} + 11.05$; the dashed line represents the locus of $L_{th} = L_{nt}$.

manages to rival with the non-thermal one. The fact that weak-lined blazars, which are normally less powerful than strong-lined ones, have a very weak, if any, thermal component, and therefore lie significantly off the correlation, would then suggest a dichotomy between the two classes.

As regards the other two bands, we also find a slope less than 1 for the correlation between the two powers, namely $L_{th} \propto L_{nt}^{0.74 \pm 0.11}$ and $L_{th} \propto L_{nt}^{0.53 \pm 0.15}$ for $7.08 \times 10^{14} - 7.24 \times 10^{14}$ Hz range and the $2.24 \times 10^{15} - 2.29 \times 10^{15}$ Hz range respectively. In both cases the significance of the $L_{th} - L_{nt}$ correlation is very high (99.8 and 99.7 per cent) once the redshift dependence is subtracted off but becomes low ($P \sim 78$ and 92 per cent) once the effect of the optical power is also considered.

6 THE DISC AND JET POWERS

In the last section we evaluated the thermal component in the optical/UV band, subtracted it from the total power and computed the ratio L_{th}/L_{nt} of monochromatic luminosities for some fixed frequencies. This led us to recognize that our sources’ optical/UV spectra are almost all dom-

inated by non-thermal emission. However, we still do not know which of the two outputs dominates the *total* power. This is because: 1) the non-thermal emission is amplified by the beaming effect; 2) the total radiative power is only a fraction of the total power in the jet; 3) the peak of the thermal luminosity (located in the UV - soft X-ray band) does not fall in the region covered by the available spectra, and thus thermal emission may overcome the non-thermal one (which is usually described by $L_{nt}(\nu) \propto \nu^{-\alpha}$, $\alpha > 0$) at higher frequencies.

For this reason we want to compare directly the total powers from the disc and jet; in the following these powers are referred to as L_{Th} and L_{Jet} , with the first letter of each subscript in upper case, to indicate that these quantities are powers integrated over the whole spectral range and not luminosities per unit of frequency as in the previous section. L_{Th} can be easily calculated by simple integration over the thermal spectra previously computed and is also basically equal to the ionizing power L_{ion} . The latter one is not easy to evaluate, however, because of beaming effects. We follow Willott et al. (1999) and define the time-averaged jet power as the total energy transported from the central engine by both jets divided by the age of the radio source. Willott et al. (1999) have derived this relationship to evaluate the jet power from the monochromatic luminosity at 151 MHz,

$$L_{Jet} \simeq 3 \cdot 10^{38} c L_{151}^{6/7} W, \quad (10)$$

where L_{151} is in units of $10^{28} \text{ W Hz}^{-1} \text{ sr}^{-1}$ and c is a factor which takes into account all the uncertainties of the calculation and lies in the range $\sim 1 - 20$. In particular, these uncertainties reside in: (i) the volume filling factor of the synchrotron emitting material; (ii) the contribution to the energy budget from protons; (iii) the dimension of the reservoir of mildly relativistic electrons; (iv) the departure from the minimum-energy condition in the lobe material. Relation (10) holds if L_{151} is the unbeamed radio luminosity, that is, the extended component of the emission at 151 MHz. As we only have measurements for the radio luminosity at 5 GHz, to estimate the jet power we need to extrapolate to 151 MHz.

The unbeamed power at 151 MHz can be expressed as follows:

$$L_{151,ub} = L_{5,ub} \left(\frac{151}{5000} \right)^{-\alpha_{ub}} \equiv \frac{L_{5,b}}{R_5} \left(\frac{151}{5000} \right)^{-\alpha_{ub}}; \quad (11)$$

where α_{ub} is the spectral index of the unbeamed component, $L_{5,b}$ and $L_{5,ub}$ are the 5 GHz powers of the beamed and unbeamed component, respectively, and R_5 is the core dominance parameter at 5 GHz.

We do not have R_5 values for all our sources. However, as the radio spectral index is a beaming indicator, we expect a relation to hold between R_5 and α_r . To derive this relation we use all FSRQ and SSRQ (steep spectrum radio quasars) in the DXRBS database for which both R_5 and α_r are available (65 sources). The correlation we find is the following:

$$\log R_5 = -(0.65 \pm 0.16) \alpha_b + 0.84, \quad (12)$$

significant at the > 99.99 per cent level. As discussed in

Landt et al. (2001), the DXRBS core-dominance parameters, based on Australia Telescope Compact Array (ATCA) data, are actually upper limits. Indeed, the same correlation for a (highly inhomogeneous) set of 49 radio-loud quasars with higher resolution radio data in the multiwavelength AGN catalog of Padovani, Giommi & Fiore (1997) yields a best-fit correlation with a slope of -0.88 ± 0.21 , consistent within the errors with ours, but with a lower intercept value. The best-fit value at $\alpha_r = 0.18$, the mean for the DXRBS sample, is in fact a factor ~ 4 smaller. In the following we then adopt the relation given by eq. (12) but with an intercept of 0.24, so that our slope comes from an homogeneous set of data. Note that this revised correlation gives a dividing value between core-dominated ($R_5 > 1$) and lobe-dominated ($R_5 < 1$) sources of $\alpha_r \sim 0.4$, not too far from the generally adopted distinction between FSRQ and SSRQ ($\alpha_r = 0.5$).

Thus, assuming $\alpha_{ub} = 0.8$, a typical value for the radio spectral index of the Fanaroff-Riley II (FR II) radio galaxies, and since $L_{5,b}/R_5 = L_5/(R_5 + 1)$, we can evaluate $L_{151,ub}$. Namely:

$$L_{151,ub} = \frac{L_5 \left(\frac{151}{5000} \right)^{-0.8}}{(10^{-0.65 \alpha_r + 0.24} + 1)}. \quad (13)$$

Figure 5 plots L_{Th} vs. L_{Jet} , with L_{Jet} calculated using $c = 20$ in eq. (10). We find that the two powers are correlated, albeit with a large scatter. Namely, $\log L_{Th} = 0.85 \log L_{Jet} + 6.69$ (the intercept becomes 7.80 if $c = 1$), $R = 0.67$, $P > 99.99$ per cent. The correlation still holds if the common redshift dependence is subtracted off ($R = 0.40$, $P = 99.99$ per cent).

Figure 6 shows the distribution of the thermal to jet power, $\log L_{Th}/L_{Jet}$, for our sample using $c = 20$ in eq. (10) (bottom axis) and $c = 1$ (top axis). The mean value for the two cases are, respectively, -0.01 ± 0.05 and 1.29 ± 0.05 or $\langle L_{Th}/L_{Jet} \rangle \sim 1$ and 20.

As a check of our method for evaluating the bolometric thermal output from the accretion disc we have used another relation in Willott et al. (1999), namely $L_{Th} \simeq 5 \times 10^3 L_{[O \text{ II}]}$, where $L_{[O \text{ II}]}$ is the power of the [O II] narrow line. This is based on assuming an equivalent width of 10 \AA for [O II], which allows an estimate of the blue luminosity, which is then converted to bolometric, under the assumption that the bolometric output is dominated by the accretion disc emission. We have estimated $L_{[O \text{ II}]}$ for our sources using the correlation with L_{151} found by Willott et al. (1999) for FR II radio sources. We find that the thermal bolometric luminosity evaluated from the relations of Willott et al. (1999), $L_{Th,2}$, is very well correlated ($R \sim 0.6$, $P \sim 99.99$ per cent) with that derived with our method, $L_{Th,1}$, albeit with a very large scatter, with a mean ordinary least-squares (OLS) slope (Isobe et al. 1990) of 1.0. The mean values for the two powers are $\langle \log L_{Th,1} \rangle = 45.44 \pm 0.07$ and $\langle \log L_{Th,2} \rangle = 45.34 \pm 0.06$. The two means and distributions are not significantly different according to a Student's t-test and a KS test respectively. We note that our method is more robust as we employ more than one emission line and no assumption on the equivalent width is made. This comparison, nevertheless, provides independent evidence that the method we use to compute the bolometric thermal power is reliable.

Finally, we want an independent method to evaluate

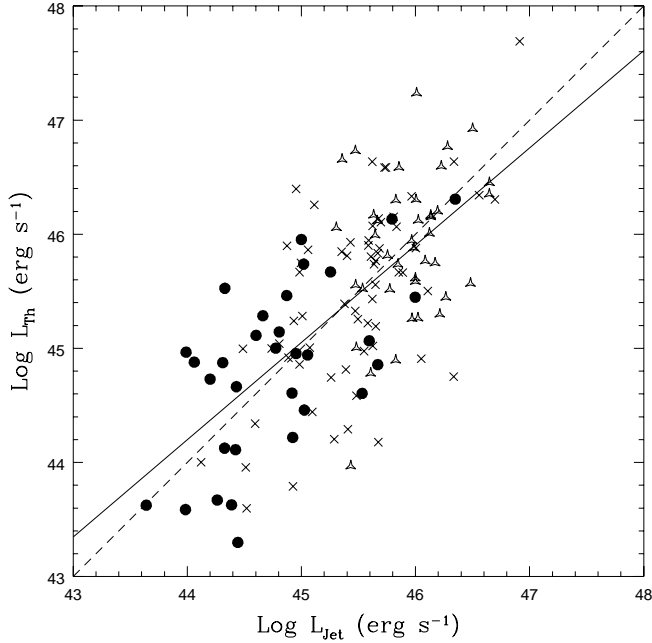


Figure 5. The relation between thermal and jet power using $c = 20$ in eq. (10). Filled circles (open triangles) represent sources whose mass has been evaluated using the $H\beta$ (C IV) line, and crosses are objects whose mass has been inferred from the correlation shown in Fig. 1. The solid line represents our best fit to the data; the dashed line represents the locus of $L_{Jet} = L_{Th}$.

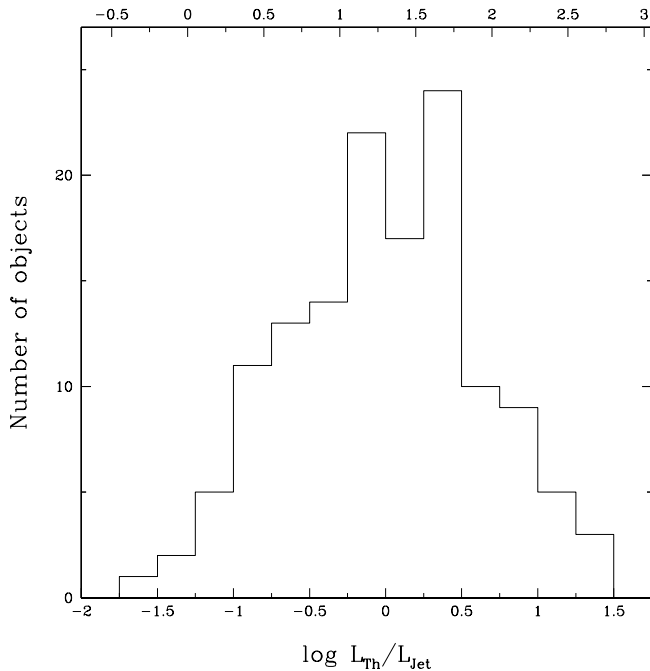


Figure 6. The ratio of thermal to jet power for our sample. The bottom axis gives the range using $c = 20$ in eq. (10), while the top axis shows the range for $c = 1$.

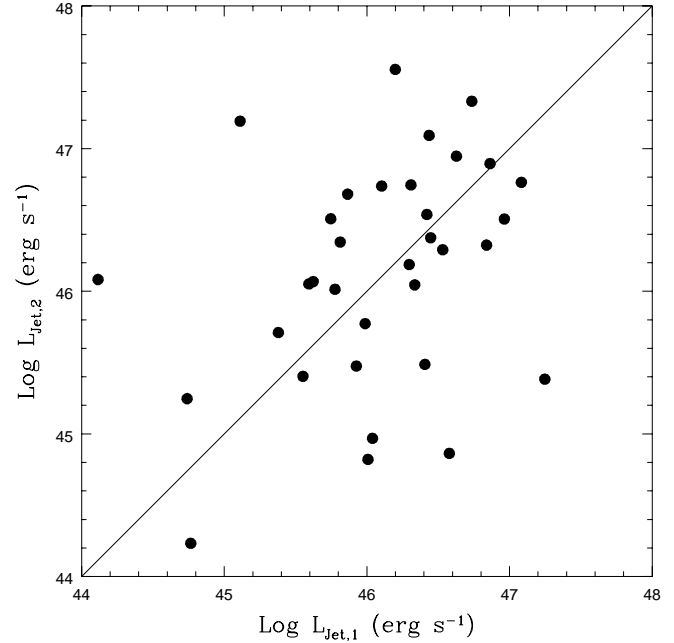


Figure 7. The comparison of the jet powers published in Celotti et al. (1997) ($L_{Jet,2}$) with those computed with eq. (10) assuming $c = 20$ ($L_{Jet,1}$) for the 34 FSRQ studied by these authors. The solid line represents the locus of $L_{Jet,1} = L_{Jet,2}$.

the jet power, for comparison with eq. (10). Celotti et al. (1997) give the jet power for 34 objects (19 high polarized, core dominated quasars and 15 low polarized, core dominated quasars), based on a synchrotron self-Compton model (SSC), applied to the radio (Very Large Baseline Interferometry [VLBI]) and X-ray fluxes. Their core dominance parameter R_5 can be found in Ghisellini et al. (1993). We then collected from the literature the luminosities at 5 GHz and used eq. (11) with $\alpha_{ub} = 0.8$ to compute the jet power and make a comparison. The results are shown in Fig. 7, where $L_{Jet,1}$ is the jet power evaluated using eq. (10) with $c = 20$ and $L_{Jet,2}$ is the jet power given in Celotti et al. (1997). We note that, despite the large scatter, the two powers are correlated ($P \sim 95$ per cent), with a mean OLS slope of 0.94. The mean values of the two sets of measurements are $\langle \log L_{Jet,1} \rangle = 46.1 \pm 0.1$ and $\langle \log L_{Jet,2} \rangle = 46.1 \pm 0.1$, i.e., the maximum powers evaluated with eq. (10) are consistent with those published in Celotti et al. (1997). This good agreement favours a large value of c .

The study of the underlying correlations between L_{Th} , L_{Jet} , and their ratio with effective spectral indices (radio-optical α_{ro} , optical-X-ray α_{ox} , and radio-X-ray α_{rx} , defined between the rest-frame frequencies of 5 GHz, 5,000 Å, and 1 keV) and powers is complicated by the very strong $L_{Jet} - L_r$ correlation which is built in due to the way we derived L_{Jet} . We studied the correlation matrix of L_{Th} , L_{Jet} , L_r , L_o , L_x plus redshift to assess which ones are the strongest correlations. Note that, whenever X-ray flux is involved, we have excluded sources with *ROSAT* Position Sensitive Proportional Counter (PSPC) offsets between 13' and 24'. This area of the PSPC, in fact, is affected by the supporting structure of the instrument, which attenuates the X-ray flux. We do not

address here correlations between radio, optical, and X-ray powers. The only significant primary (non-trivial) correlations are $L_{Th} - L_o$ and $L_{Th} - L_x$. All correlations involving L_{Jet} are secondary and due to the $L_{Jet} - L_r$ correlation. No correlations are present between L_{Jet} and the effective spectral indices once the effect of L_r is taken into account. On the other hand, L_{Th} correlates with α_{ro} (negatively) and α_{ox} (positively). The L_{Th}/L_{Jet} ratio anti-correlates strongly with α_{ro} and α_{rx} , but the latter correlation appears to be induced by the former.

To conclude, we now discuss how our results would change for different choices of covering factor and black hole. If a covering factor of ~ 30 per cent instead of 10 per cent is assumed all the computed thermal powers decrease roughly by a factor ~ 3 . The dominance of the non-thermal emission in the optical/UV would become even stronger, as the thermal component would only make up ~ 7 per cent of the power. The average ratio between the total disc and the jet power would be ~ 0.3 (~ 7) for $c = 20$ ($c = 1$). In this case, our thermal powers would be on average a factor ~ 2 below those estimated using the Willott et al. correlations. Assuming a non-rotating black hole would increase the accretion rates by a factor ~ 5 , as the efficiency goes down but the ionizing power is fixed by the BLR power (see eq. 8). The shape of the spectrum also changes because the radius of the last stable orbit increases. The combination of these two effects result in a thermal spectrum which is not too different from that of a rotating black hole, with a slight shift towards lower frequencies and a slightly higher normalization.

7 DISCUSSION

Three main results have come out of this work. We discuss them now in turn.

7.1 The Thermal Component in the Optical/UV Spectra of Flat-spectrum Radio Quasars

It has long been thought that any thermal emission related to accretion in the optical/UV spectra of FSRQ had to be relatively weak, or rather swamped by the non-thermal emission from the jet (although exceptions exist, e.g., 3C 273). We have quantified this in a systematic, albeit model-dependent way, by deriving an accretion disc spectrum and by then comparing it to the observed rest-frame optical/UV spectra of more than 100 FSRQ from the DXRBS. The determination of the mass and accretion rate for our sources, which are required parameters of the model, should be relatively robust. The former is based on the virial theorem, by now widely used, normalized on the results of reverberation mapping campaigns. (Even the mass determinations based on C IV agree very well with a recent calibration published by Vestergaard (2002).) The latter has been derived from the BLR power and the only uncertainty there is the covering factor, which we think should be constrained within a factor ~ 3 . Moreover, the reliability of our method has been tested by comparing the predictions of the model with the observed optical/UV spectra of a sample of radio-quiet quasars, under the assumption that in this case most of the emission should be due to the disc. Reassuringly, the predictions were within a factor of two from the observations.

We have found that the optical/UV emission of FSRQ is dominated by a non-thermal component, which makes up ~ 85 per cent of the total power. Only in a small fraction ($\lesssim 9$ per cent) of the objects does the thermal component dominates. This is consistent with the relatively steep optical/UV slopes of DXRBS FSRQ ($\alpha \sim 1.2$; Landt et al., in preparation). In all three rest-frame bands we have used there is evidence that the thermal fraction is higher at lower non-thermal powers, which might suggest that only in less powerful, and therefore possibly less beamed, sources the thermal component manages to rival with the non-thermal one.

Whiting, Webster & Francis (2001) have fitted the optical and near-infrared SEDs of ~ 100 FSRQ from the Parkes Half-Jansky flat-spectrum sample. They assessed the relevance of thermal and non-thermal components by fitting a blue power law (fixed to $\alpha_B = 0.3$) and optical synchrotron emission. The ratio of the synchrotron and power-law components at a rest-frame wavelength of 5,000 Å was found to span nearly four orders of magnitude. The distribution was strongly peaked, however, at ratios $\gtrsim 10$, suggesting a dominance of non-thermal emission in the optical band of these sources, in agreement with our results obtained with an independent method.

7.2 The Masses of Radio-loud Quasars

It has been suggested in the literature that radio-loud quasars require massive black holes. Laor (2000) pointed out that nearly all Palomar-Green (PG) quasars with $M > 10^9 M_\odot$ are radio-loud, while quasars with $M < 3 \times 10^8 M_\odot$ are practically all radio-quiet. This has been recently taken up by Boroson (2002), who has suggested a scheme to explain the radio-loud/radio-quiet dichotomy based on mass and Eddington ratio. Ho (2002), however, by using a sample which spanned a large range of activity, did not confirm the trend found by Laor (2000). Lacy et al. (2001) also found a dependence of black hole mass on the radio-loudness parameter R^* (equivalent to our α_{ro}) with most radio-loud ($R^* > 10$) sources having $M >$ a few $\times 10^8 M_\odot$, but with the radio-quiet ones extending to $\gtrsim 10^9 M_\odot$.

About 25 per cent of our sources, which are all strongly radio-loud ($\langle \alpha_{ro} \rangle \sim 0.65$, well above the typically assumed dividing line of 0.2), have $M < 3 \times 10^8 M_\odot$. If we restrict ourselves to the objects whose mass has been derived from $H\beta$, for comparison with previous studies, this fraction gets much higher. The mean mass in this case is $\langle \log M \rangle = 8.41 \pm 0.09 M_\odot$ (to be compared with $\langle \log M \rangle = 8.74 \pm 0.04 M_\odot$ for the whole sample) and now ~ 47 per cent of our objects have estimated black hole masses below $3 \times 10^8 M_\odot$. Keeping in mind the danger of comparing results for samples selected with different criteria, the mass range covered by our radio-loud quasars is not very different from that of the radio-quiet quasars in Laor (2000).

If the motion of emission-line gas is confined predominantly to a disc perpendicular to the radio axis then in core-dominated (flat-spectrum) sources, like ours, we might be biased towards low FWHM values (Wills & Browne 1986) and, therefore, we might be underestimating the black hole masses. Although this could have some effect on our results, we believe it cannot be major (see also Oshlack et al. 2002). First, within DXRBS we do not find any corre-

lation between $\text{FWHM}(H\beta)$ (and also $\text{FWHM}(C\ IV)$) and α_r , although the relative number of SSRQ in DXRBS is, by construction, small (~ 24 per cent and ~ 18 per cent for sources with $H\beta$ and C IV respectively), as we have a cut at $\alpha_r \leq 0.7$. We also do not find any correlation between ATCA core-dominance parameter and $\text{FWHM}(H\beta)$ (20 sources) or $\text{FWHM}(C\ IV)$ (27 sources). Second, Gu, Cao & Jiang (2001) have assembled $\text{FWHM}(H\beta)$ for 86 radio sources, selected from the 1 Jy, S4, and S5 catalogs, including 55 FSRQ and 31 SSRQ. Table 2 in Oshlack et al. (2002) shows that the ratio of the mean (median) $\text{FWHM}(H\beta)$ for SSRQ and FSRQ is ~ 1.44 (~ 1.25), which would imply a “correction” factor for our $H\beta$ masses ~ 2 (~ 1.6). This means that ~ 28 per cent of our low-redshift objects would still have estimated black hole masses below $3 \times 10^8 M_\odot$. As discussed in Sect. 4, a factor of 2 increase in black hole mass has in any case a small effect on our other results.

Oshlack et al. (2002) have estimated black hole masses for 39 sources belonging to the Parkes Half-Jansky flat-spectrum sample, also finding that a significant fraction of the radio quasars in their sample have relatively small masses. Both studies are based on complete, radio-selected samples so the failure of some previous studies to find radio-loud quasars with small masses is likely due to a selection effect. Oshlack et al. (2002) comment on the fact that there is a strong correlation between mass and optical/UV luminosity, shown for our sample in Fig. 1, a consequence of using ionizing power to estimate the BLR radius. This implies that if a sample is biased against selecting low optical luminosity, radio-loud quasars, as seems to be the case for the PG sample, it will miss the low-mass radio-loud sources. DXRBS is almost completely identified and we find a large range of optical powers in our quasar sample.

Contrary to what found by Laor (2000), we find an anti-correlation between mass and α_{ro} , in the sense that the most radio-loud sources have also the smaller masses. Again, this is partly induced by the correlations between mass and ionizing (optical) power and α_{ro} and optical power (see also Oshlack et al. 2002).

The relationship between black hole mass and radio power has also been recently addressed in the literature. Since all our sources have a radio flat-spectrum and are therefore heavily affected by relativistic beaming, we cannot comment on this point.

7.3 The Disc - Jet Connection in Flat-spectrum Radio Quasars

Even more interesting than the non-thermal/thermal ratio in the optical/UV band is the relationship between integrated disc and jet emission. The former is easily derived assuming that the ionizing photons originate in the accretion disc and therefore depends on the BLR luminosity and the covering factor. Note that the total disc emission is independent of the mass. An estimate of the total jet power is more difficult to obtain, because it depends on many astrophysical parameters, some of which are at present not well constrained. We have then relied on the theoretical relationship obtained by Willott et al. (1999), which links jet power to the extended radio emission at 151 MHz, derived for our sources from their 5 GHz radio power and radio spectral in-

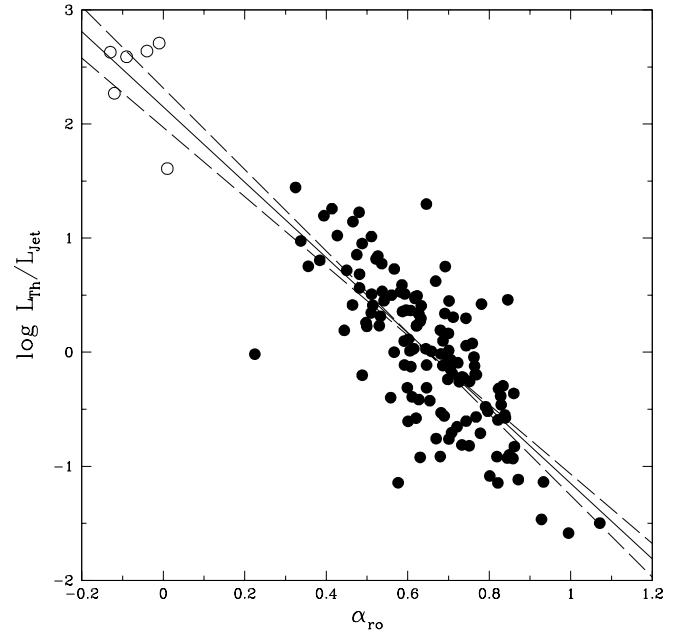


Figure 8. The ratio of thermal to jet power (using $c = 20$ in eq. 10) vs. α_{ro} . Filled circles represent our FSRQ while open circles represent the subset of radio-quiet quasars in Tab. 2 with extended radio power information. The solid line represents the best fit to the FSRQ data, while the dashed lines indicate the 1σ dispersion. See text for details.

dex. This relationship has a built-in uncertainty ~ 20 , due to various uncertainties in the model assumptions.

We compared the results of both estimates to previous results obtained using independent methods, with relatively good agreement. In particular, an application of our method to estimate jet power to the 34 quasars studied by Celotti et al. (1997) using an SSC model favours large values of c and would actually suggest a nominal value $c \sim 20$.

We have found that $L_{Th} \propto L_{Jet}^{0.9}$ and that, on average, $L_{Th}/L_{Jet} \sim 1$ (or 20 if $c = 1$). The dispersion around the average is relatively large, about a factor of 4 (1σ). This could simply reflect the uncertainties of our method or might indicate a dependence of this ratio on some parameter. One of the strongest correlations we find is between L_{Th}/L_{Jet} and the optical-to-radio flux ratio, which we parametrize using α_{ro} . This correlation might be expected given that $L_{Th} \propto L_o$ and $L_{Jet} \propto L_r$. (We note however that we have shown that L_o is dominated by the non-thermal component, while L_{Jet} depends by construction on the extended radio emission, while our sources are mostly core-dominated.) However, it is not induced by other correlations and therefore might be used to estimate the total disc to jet power ratio as a function of radio-loudness.

Fig. 8 plots L_{Th}/L_{Jet} (using $c = 20$ in eq. 10) vs. α_{ro} for our sources. The best fit is $\log L_{Th}/L_{Jet} = -(3.30 \pm 0.26)\alpha_{ro} + 2.15$. (The intercept value becomes 3.45 if $c = 1$ is used instead.) Assuming that this relationship can be extrapolated to the radio-quiet regime, we get $L_{Th}/L_{Jet} \sim 200$ for $\alpha_{ro} \sim -0.05$, a value typical for radio-quiet AGN. (If $c = 1$ we get instead $L_{Th}/L_{Jet} \sim 4,000$.) We checked this extrapolation by estimating the jet power for the radio-quiet

(PG) quasars used in Sect. 4 to test our accretion disc model. Namely, we derived the extended radio flux at 5 GHz for the sources in Tab. 2 by subtracting the core from the total fluxes given in Kellermann et al. (1989). Only the six sources for which this difference was larger than the quoted noise summed in quadrature (0.09 mJy) were considered. The flux was then extrapolated at 151 MHz assuming a radio spectral index of 0.8 and then eq. (10) was used to estimate the jet power. The radio-quiet quasars fall on the extrapolation of the relation obtained for the FSRQ in the $L_{Th}/L_{Jet} - \alpha_{ro}$ plane. This supports the use of α_{ro} to estimate the disc to jet power ratios in all broad-line AGN and suggests that the disc to jet power ratio in radio-quiet AGN is a few hundred times larger than in radio-loud AGN. The disc power for the two classes, at least for the sources discussed in this paper, is comparable, so what is changing is obviously jet power.

Note that in both classes of sources the contribution of the host galaxy to the optical emission (and therefore to α_{ro}) is negligible. The DXRBS FSRQ are typically at $z \sim 1.5$, where the strong nuclear luminosity evolution should make the AGN dwarf the host galaxy. As regards the PG quasars, these were selected on the basis of being “point-like”. Detailed imaging studies (e.g., McLeod & McLeod 2001) have indeed confirmed that the ratio of host to nuclear light is $\ll 1$ in the near-infrared band, and therefore even smaller in the optical.

7.3.1 Comparison with Previous Results

We now want to compare our results with previous works also aimed at studying the relation between thermal and jet power in radio-loud sources.

Rawlings & Saunders (1991) found a very strong correlation, covering four orders of magnitude, between the jet kinetic power and narrow line region luminosity in radio-loud objects. Since the power of the narrow line region is proportional to the thermal power, this translates in a correlation between the latter and the jet power, similar to ours. The slope of our correlation is close to that of Rawlings & Saunders (1991), and their average ratio between thermal and jet power is close to unity (we find an average value of ~ 1 , for $c = 20$), even if their computation of the kinetic power is carried out in a different way, i.e., by invoking equipartition between the magnetic field and the electron energy densities in the jets.

Celotti et al. (1997) found a weak (95.8 per cent) correlation between the jet kinetic energy and the power of the broad line region for an inhomogeneous sample of radio-loud sources composed of Steep Spectrum Radio Quasars, FSRQ, and BL Lacertae objects, with the thermal and jet powers of the same order of magnitude.

Willott et al. (1999) evaluated the relation between the thermal and non-thermal power for a very large sample of FR II radio sources. We have adopted their method to estimate jet power but they evaluated the thermal power from the [O II] line luminosity. They found an average thermal to jet power ratio $\sim 1 - 2$ for $c = 20$ depending on the cosmology adopted ($q_0 = 0.5$ and $q_0 = 0$, respectively) and $20 - 40$ for $c = 1$. The values we find for our FSRQ sample are ~ 1 and 20 (see also Fig. 6), consistent within a factor of two. Thus, we can conclude that our blazars behave as their parent population, the FR II radio galaxies, and this is def-

initely in favour of unified scheme models (Scheuer 1987; Barthel 1989; Antonucci 1993; Urry & Padovani 1995).

Maraschi & Tavecchio (2002) estimated the jet power for 11 FSRQ using synchrotron inverse-Compton fits to multiwavelength data and the accretion power for the same objects using the optical-UV bump in their data or the BLR luminosity when the data did not feature such a bump. In agreement with Celotti et al. (1997), they found that the two powers are of the same order of magnitude.

7.3.2 Jet Models

The leading model to explain jet production is the Blandford & Znajek (1977; BZ) mechanism, that involves the electrodynamic extraction of rotational energy from a spinning black hole (i.e., a Kerr hole). The BZ power scales as

$$L_{BZ} \propto r^2 B^2, \quad (14)$$

r being the radius of the Kerr hole and B being the magnetic field threaded to the hole (see also Cavaliere & D’Elia 2002 for a detailed discussion). However, the BZ mechanism has been proven to be insufficient to achieve the luminosities of the most powerful FSRQ due to the magnetic field, which is limited by the radiation pressure in the accretion disk. Ghosh & Abramowicz (1997), for example, have shown that in a radiation pressure dominated disk, the *maximum* value of the electromagnetic energy that can be extracted from the Kerr hole is

$$L_K \approx 2 \cdot 10^{45} M_9 a^2 \text{ erg s}^{-1}, \quad (15)$$

where M_9 is the Kerr hole mass in units of $10^9 M_\odot$ and the parameter a describes the rotation of the hole ($a = 1$ for a maximally spinning hole and $a = 0$ for a non-rotating black hole). We can see from eq. (15) that the jet power in our most luminous FSRQ, which can reach almost 10^{47} erg s^{-1} (see Fig. 5), cannot be explained using the BZ mechanism to extract energy from the Kerr hole, even assuming the highest mass we have estimated for our sources $\sim 8 \times 10^9 M_\odot$ (see also Maraschi & Tavecchio 2002). For our sample we can calculate L_K using eq. (15) and the black hole masses we evaluated and compare it with the jet power computed from eq. (10) with $c = 20$. We find that, while $\langle \log L_{Jet} \rangle = 45.45 \pm 0.06$, $\langle \log L_K \rangle = 45.04 \pm 0.04$, i.e., a factor ~ 3 smaller. Thus, on average, even the *maximum* Kerr hole luminosity produced via the BZ mechanism is not able to explain the estimated L_{Jet} , although in ~ 24 per cent of our objects L_K is greater than L_{Jet} . Note that for a value of $c = 1$ we get $\langle \log L_{Jet} \rangle = 44.14 \pm 0.06$, 8 times *smaller* than L_K , with L_K greater than L_{Jet} for ~ 94 per cent of the objects. But in this case our jet power estimates would be in gross disagreement with previous derivations. The point remains, however, that the difference we find between jet and maximum BZ power is smaller than that found, for example, by Maraschi & Tavecchio (2002; see their Fig. 3). We attribute this to the fact that DXRBS is sampling FSRQ of lower power than the “classical”, high-power ones normally studied.

To explain the jet power in FSRQ two variants of the BZ process has been proposed. The first one invokes the electrodynamic extraction of rotational energy from the accretion disk too (Blandford & Payne 1982). This basically corresponds to using a larger value for r in eq. (14). The second

variant argues for strong magnetic fields in the plunging orbit region, where relativistic effects could enhance such fields to higher values than those fixed by the radiation pressure in the accretion disk (e.g., Meier 1999). Further investigations are definitely needed in order to shed more light on the BZ process and on its role in the production of blazar jets.

8 SUMMARY AND CONCLUSIONS

We have presented an indirect approach to investigate the relationship between accretion disc and jet in strong-lined blazars. As the luminosity produced from the accretion disc in the optical/UV band cannot be observed directly because of the beamed jet emission, we have estimated the disc component using an accretion disc model for 136 flat-spectrum radio quasars. These sources belong to the Deep X-ray Radio Blazar Survey (DXRBS) and therefore represent a well-defined, almost completely identified sample. The model requires an estimate of the mass and accretion rate for each source. These have been derived from broad line widths, normalizing our BLR distances to the results of reverberation mapping campaigns, and ionizing powers, the latter derived from the BLR power, which we derive from the emission line fluxes, mostly from our own spectra. Our estimate of the thermal component has been tested for a sample of radio-quiet quasars, for which the thermal component should dominate. Indeed, the observed powers at the predicted peak of the thermal emission were within a factor less than two from those computed with our method.

Our main results can be summarized as follows:

(i) The application of our method to the observed spectra of our sources has shown that non-thermal emission dominates the (rest-frame) optical/UV band of strong-lined blazars, accounting on average for ~ 85 per cent of the power. Only a small fraction ($\lesssim 10$ per cent) of our flat-spectrum radio quasars shows a dominance of thermal emission in their optical/UV spectra.

(ii) The ratio between *integrated* disc and jet power is, on average, $\gtrsim 1$, possibly reaching typical values as high as 20. This large range is due to uncertainties in the assumptions that have gone into the relation we have used to estimate jet power from extended radio power, derived by Willott et al. (1999). Nevertheless, a comparison with results from an SSC-based method favours low values for this ratio. We have used the correlation between disc-to-jet power ratio and optical-to-radio flux ratio to estimate that the former parameter is a few hundred times larger in radio-quiet AGN than it is in radio-loud AGN. This is confirmed by estimating the jet power for a handful of radio-quiet quasars.

(iii) A by-product of our study is an estimate of black hole masses for radio quasars belonging to a well-defined sample. Contrary to some previous studies, we have found that a sizeable fraction of our sample (~ 25 per cent; 50 per cent of the $H\beta$ sample) has a relatively small ($M < 3 \times 10^8 M_\odot$) mass, which argues that radio-loud sources do not require particularly massive black holes. Eddington ratios are typically ~ 0.1 .

(iv) We have calculated the maximum power that can be extracted from a rotating black-hole in our sources according to the Blandford-Znajek mechanism, making use of our mass estimates. If the jet power is as high as inferred by a

comparison with independent methods, it can be explained by the Blandford-Znajek process only in a minority (~ 25 per cent) of our sources.

ACKNOWLEDGEMENTS

This work has been partially supported by the STScI (DDRF) grant D0001.82274. We thank the referee for helpful comments.

REFERENCES

- Anderson T. W., 1984, *An Introduction to Multivariate Statistical Analysis*. Wiley, New York
- Antonucci R. R. J., 1993, *ARA&A*, 31, 473
- Band D. L., Malkan M., 1989 *ApJ*, 345, 122
- Barthel P. D., 1989, *ApJ*, 336, 606
- Blandford R. D., Payne D. G., 1982, *MNRAS*, 199, 883
- Blandford R. D., Rees M., 1978, in Wolfe A. N., ed., *Pittsburgh Conference on BL Lac Objects*, p. 328
- Blandford R. D., Znajek R., 1977, *MNRAS*, 179, 433
- Boettcher M., 2000 in *AIP*, Vol. 515, p. 31
- Boroson T. A., 2002, *ApJ*, 565, 78
- Cavaliere A., D’Elia V., 2002, *ApJ*, 571, 226
- Celotti A., Padovani P., Ghisellini G., 1997, *MNRAS*, 286, 415
- Czerny B., Elvis M., 1987, *ApJ*, 321, 305
- Elvis M., Fiore F., Siemiginowska A., Bechtold J., Mathur S., McDowell J., 2000, *ApJ*, 543, 545
- Filippenko A. V., 1982, *PASP*, 94, 715
- Forster K., Green P. J., Aldcroft T. L., Vestergaard M., Foltz C. B., Hewett P. C., 2001, *ApJS*, 134, 35
- Fossati G., Maraschi L., Celotti A., Comastri A., Ghisellini G., 1998, *MNRAS*, 299, 433
- Francis P. J., Hewett P. C., Foltz C. B., Chaffee F. H., Weymann R. J., Morris S. L., 1991, *ApJ*, 373, 465
- Fromerth M. J., Melia F., 2000, *ApJ*, 533, 172
- Ghisellini G., 1999, *Astroparticle Physics*, 11, 11
- Ghisellini G., Padovani P., Celotti A., Maraschi L., 1993, *ApJ*, 407, 65
- Ghosh P., Abramowicz M., 1997, *MNRAS*, 292, 887
- Gu, M., Cao, X., Jiang, D. R., 2001, *MNRAS*, 327, 1111
- Ho L. C., 2002, *ApJ*, 564, 120
- Isobe T., Feigelson E. D., Akritas M. G., Babu G. J., 1990, *ApJ*, 364, 104
- Jorstad S. G., Marscher A. P., Mattox J. R., Wehrle A. E., Bloom S. D., Yurchenko A. V., 2001, *ApJS*, 134, 181
- Kaspi S., Smith P. S., Netzer H., Maoz D., Jannuzi B. T., Giveon U., 2000, *ApJ*, 533, 631
- Kellermann K. I., Sramek R., Schmidt M., Shaffer D. B., Green R., 1989, *AJ*, 98, 1195
- Kendall M., Stuart A., 1979, *The Advanced Theory of Statistics*. MacMillan, New York
- Kriss G. A., Davidsen, A. F., Zheng W., Lee G., 1999, *ApJ*, 527, 683
- Lacy M., Laurent-Muehleisen S. A., Ridgway S. E., Becker R. H., White R. L., 2001, *ApJ*, 551, L17
- Landt H., Padovani P., Perlman E. S., Giommi P., Bignall H., Tzioumis A., 2001, *MNRAS*, 323, 757
- Laor A., Fiore F., Elvis M., Wilkes B. J., McDowell J. C., 1997 *ApJ*, 477, 93
- Laor A., 2000, *ApJ*, 543, L111
- Maiolino R., Salvati M., Marconi A., Antonucci R. R. J., 2001, *A&A*, 375, 25
- Malkan M. A., 1982, *ApJ*, 268, 582
- Maraschi L., Tavecchio F., 2002, *ApJ*, in press (astro-ph/0205252)

- McLeod K. K., McLeod B. A., 2001, *ApJ*, 546, 782
- McLure R. J., Dunlop J. S., 2001, *MNRAS*, 327, 199
- Meier D. L., 1999, *ApJ*, 522, 753
- Misner C., Thorne K., Wheeler J., 1970, *Gravitation*. W. H. Freeman and Company, San Francisco
- Moderski R., Sikora M., Lasota J.-P., 1998, *MNRAS*, 301, 142
- Mukherjee R., 2001, in Aharonian F. A., Völk H. J., eds, *High Energy Gamma-Ray Astronomy*, AIP, Vol. 558, p. 324
- Netzer H., 1990, in Courvoisier T. J.-L., Major M., eds, *Active Galactic Nuclei, Saas-Fee Advanced Course 20*. Springer-Verlag, Berlin, p. 57
- Oshlack A. Y. K. N., Webster R. L., Whiting M., 2002, *ApJ*, 576, 81
- Padovani P., Giommi P., Fiore F., 1997, *Mem. Soc. Astron. Italiana*, 68, 147
- Perlman E. S., Padovani P., Giommi P., Sambruna R., Laurence R. J., Tzioumis A., Reynolds J., 1998, *AJ*, 115, 1253
- Peterson B. M., 1993, *PASP*, 105, 247
- Pringle J. E., 1981, *Ann. Rev. Astron. Astrophys.* 19, 137
- Rawlings S., Saunders R., 1991, *Nature*, 349, 138
- Scheuer P. A. G., 1987, in Zensus J. A., Pearson T. J., eds, *Superluminal Radio Sources*. Cambridge Univ. Press, Cambridge, p. 331
- Shakura N. I., Sunyaev R. A., 1973, *A&A*, 24, 337
- Urry C. M., Padovani P., 1995, *PASP*, 107, 83
- Vestergaard M., 2002, *ApJ*, 571, 733
- Wandel A., Peterson B. M., Malkan M. A., 1999, *ApJ*, 526, 579
- White R. L., Giommi P., Angelini L., 1995, database at <http://wgacat.gsfc.nasa.gov>
- Whiting M. T., Webster R. L., Francis P. J., 2001, *MNRAS*, 323, 718
- Wilkes B. J., Wright A. E., Jauncey D. L., Peterson B. A., 1983, *Astr. Soc. of Australia, Proc*, 5, 2
- Willott C. J., Rawlings S., Blundell C. M., Lacy M., 1999, *MNRAS* 309, 1017
- Wills B. J., Browne I. W. A., 1986, *ApJ*, 302, 56
- Wilson A. S., Colbert E. J. M., 1995, *ApJ*, 438, 62
- Yuan M. S., Tran H., Wills B., Wills D., 2001, in Padovani P., Urry C. M., eds, *ASP Conf. Ser. Vol. 227, Blazar Demographics and Physics*. Astron. Soc. Pac., San Francisco, p. 150